INTERNATIONAL JOURNAL FOR NUMERICAL METHODS IN FLUIDS
Int. J. Numer. Meth. Fluids **29**: 555–573 (1999)

NUMERICAL SIMULATION OF A FLOW AROUND AN IMPULSIVELY STARTED RADIALLY DEFORMING CIRCULAR CYLINDER

SAMIR HANCHI[a], RADOMIR ASKOVIC[a] AND LOC TA PHUOC[b,*]

[a] *Laboratoire de Mécanique des Fluides, Université de Valenciennes et du Hainaut-Cambresis, Le Mont Houy, BP 311, 59304 Valenciennes Cedex, France*
[b] *LIMSI-CNRS, B.P. 133, 91403 Orsay, France*

SUMMARY

The development of a two-dimensional viscous incompressible flow generated by a deformable circular cylinder impulsively started into rectilinear motion is studied numerically for the Reynolds numbers equal to 550 and 3000. The vorticity transport equation is solved by a second-order finite difference method in both directions of the domains. The Poisson equation for the streamfunction is solved by a Fourier–Galerkin method in the direction of the flow that is assumed to remain symmetrical and a second-order finite difference for the radial direction. The advance in time is achieved by a second-order Adams–Bashforth scheme. The computed results are compared qualitatively with experimental and numerical results done before in the particular non-deformable case. The comparison is found to be satisfactory. The influence of the deformation of the cylinder on the flow structure and the drag coefficient is then analyzed. Copyright © 1999 John Wiley & Sons, Ltd.

KEY WORDS: numerical simulation; body deformability; viscous flow

1. INTRODUCTION

Despite the simplicity of the obstacle geometry, the flow structure around an impulsively started circular cylinder (non-deformable) into rectilinear motion is complex, and all the phenomena of fluid mechanics are present. That is why, for more than a century, numerous theoretical, computational and experimental investigations of this problem have been reported in the literature.

Theoretical investigations of an impulsively started flow were first undertaken by Blasius in 1908 [1], who obtained the first two terms of a time series solution of the boundary layer equations. Subsequently, there have been many works attempting to obtain higher-order terms and advance the solution beyond the separation stage. The authors [2–5] have all considered this problem in the limiting case of infinite Reynolds number. Some authors [6–10] have extended their works to finite and high Reynolds numbers. In [7,8], the problem is formulated in boundary layer variables and an expansion in powers of time is obtained. These expansions are corrected to take into account finite Reynolds number effects and are adjusted to match the uniform flow far from the cylinder. In [9], the vorticity equation is solved by the method

* Correspondence to: LIMSI-CNRS, B.P. 133, 91403 Orsay, France.

CCC 0271–2091/99/050555–19$17.50

Received June 1997
Revised March 1998

of matched asymptotic expansions. Inner (rotational flow) and outer (potential flow) solutions are obtained to third-order in time and a composite solution is formed. The last two works [8,9] provide extensive information for flow quantities of interest (such as vorticity field, streamlines, body forces). In [10], the unsteady boundary layer equation of second-order is solved by the parametric method of matched asymptotic expansions. All these works are valid for relatively short times and the range of validity increases with increasing Reynolds number.

The second class is that of purely numerical solutions of the Navier–Stokes equations. Chronologically, Thom [11] gave the first numerical solution of steady Navier–Stokes equations corresponding to viscous flow around a circular cylinder. Unsteady flow was first studied for Reynolds numbers equal to 40 and 100 [12]. The works [7,8,13–19] investigated this problem for different Reynolds numbers. The common points of interest of these papers are the development of the primary unsteady wake length behind the cylinder and the evolution in time of the drag coefficient and separation angle.

In all these references, the problem is formulated in vorticity–streamfunction variables, and then Eulerian, Lagrangian and hybrid methods have been used for their discretization. Numerous computations have been performed over the past 30 years on this flow, but there are still open questions as to whether the numerics interfere with the physics of the problem, especially for the high Reynolds number flows. Ta Phuoc [20] uses a fourth-order scheme to resolve the Poisson equation for the streamfunction and a second-order finite difference scheme for the vorticity transport equation. He presented computations for a range of Re (550–1000) and detailed diagnostics and comparisons with experimental results. This work was extended to higher Re (3000–9500) [21]. Lecointe and Piquet [22] tested several high-order compact finite difference schemes as well, and they presented accurate computations for Re up to 550 and tentative simulations for higher values of Re. A more recent work is that of Wang and Dalton [23]. They used a predictor–corrector finite difference scheme for the vorticity transport equation and a fast Poisson solver for the streamfunction. They presented results for impulsively started and stopped flows for Re of 102 and 550.

More recently, some new numerical procedures, called vortex methods, are used to integrate the vorticity–velocity formulation of the Navier–Stokes equations. In vortex methods, the most notable studies are [24–26]. The first two investigations use the cloud-in cell method [27] to convect the vortices but use different techniques to take account for viscous effects. Smith and Standsby [24] used the method of random walks, whereas Chang and Chern [25] used a finite difference scheme on the grid used by the cloud-in cell technique to resolve the diffusion operator. Both works take advantage of the stability properties of vortex methods to extend their computations to very high Reynolds numbers (up to 10^6 in [25]). However, it appears that the increase in Re simulated is not followed by an adequate increase in the resolution. Recently, some researchers [28,29] have conducted simulations of this flow using finite difference schemes. Their simulations demonstrated the computational difficulties of the problem, since very large numbers of grid points were necessary, in both works, to advance the solution up to $t = 3$ for $Re = 9500$.

Koumoutsakos and Leonard [26] developed high-resolution direct numerical simulations using a novel adaptive numerical scheme, based on vortex methods. They used up to a million computational elements by efficiently implementing fast summation algorithms and by introducing a novel scheme for the enforcement of the no-slip condition for the vorticity–velocity formation of the Navier–Stokes equations. Their results, compared with some representative experimental, theoretical and computational works, provide benchmark quality simulations for the early stages of the flow around an impulsively started cylinder. Moreover, they identify the underlying mechanisms of unsteady separation and describe the effect of these phenomena on the drag coefficient.

Experimental investigations on unsteady flows resulting from an impulsive acceleration of a non-deformable cylinder date back to time of Prandtl (1925) [30]. Some experimental visualizations were described in [31,32]. However, the most extensive experiments to date seem to be those presented by Bouard and Coutanceau [33] for a translating cylinder. They analyzed in detail the topological structure (formation and development of secondary vortices) of the flow around a cylinder by using the instantaneous velocity field and streamlines.

The complex problem of unsteady viscous flow around a deformable body is of interest as well in nature as in the technical practice (self-adaptable surfaces, for instance). The relevant physical problem could be also a non-viscometric flow in contact with the wall. The present work is concerned with the analysis of the flow structure at early times of the impulsively started uniformly deforming circular cylinder. The Poisson equation for the streamfunction is solved by a Fourier–Galerkin method coupled with a finite difference method of second-order. The vorticity transport equation is solved by a second-order Adams–Bashforth procedure, similar to Hakizumwami [34], which requires neither the preliminary calculation nor the iterative process.

2. BASIC EQUATIONS

Consider the unsteady flow past a circular cylinder whose radius (of initial value a_0) grows uniformly with a constant factor of deformability A, started impulsively at the same time into rectilinear motion, with a constant velocity U_∞, in a 2D viscous incompressible fluid initially at rest. The unsteady Navier–Stokes equations in streamfunction and vorticity formulation for the flow past a circular cylinder can be written in polar co-ordinates as

$$\frac{\partial \varpi}{\partial t_1} = \frac{1}{r_1}\left[\frac{\partial}{\partial r_1}\left(\varpi \frac{\partial \psi_1}{\partial \theta}\right) - \frac{\partial}{\partial \theta}\left(\varpi \frac{\partial \psi_1}{\partial r_1}\right)\right] + \nu \nabla^2 \varpi, \tag{1}$$

with

$$\varpi = \nabla^2 \psi_1 \tag{2}$$

and

$$\nabla^2 = \frac{\partial^2}{\partial r_1^2} + \frac{1}{r_1}\frac{\partial}{\partial r_1} + \frac{1}{r_1^2}\frac{\partial^2}{\partial \theta^2},$$

where (r_1, θ) are polar co-ordinates (Figure 1), ν is the kinematic viscosity and t_1 is the time. The streamfunction ψ_1 is defined by

$$u_1 = -\frac{1}{r_1}\frac{\partial \psi_1}{\partial \theta} \quad \text{and} \quad v_1 = \frac{\partial \psi_1}{\partial r_1} \tag{3}$$

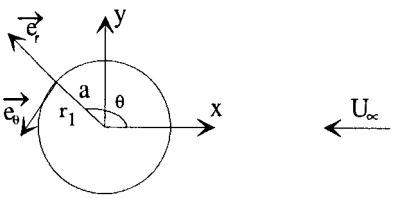

Figure 1. System of co-ordinates.

and the only non-zero component of the vorticity ϖ is

$$\varpi = \frac{1}{r_1}\left(\frac{\partial}{\partial r_1}(v_1 r_1) - \frac{\partial u_1}{\partial \theta}\right). \tag{4}$$

By introducing non-dimensional quantities,

$$\frac{a}{a_0} = (1 + At), \qquad r = \frac{r_1}{a} = \mathrm{e}^{\xi}, \qquad Re = \frac{2U_\infty a}{\nu}, \qquad t = \frac{t_1 U_\infty}{a_0}, \qquad \tilde{\psi} = \frac{\psi_1}{U_\infty a},$$

$$\omega = \frac{\varpi a}{U_\infty}, \tag{5}$$

(1) and (2) become

$$\frac{\partial \omega}{\partial t} = \frac{\omega}{a}\frac{\partial a}{\partial t} + \frac{a_0}{a}\,\mathrm{e}^{-2\xi}\left[\frac{\partial \omega}{\partial \xi}\frac{\partial \tilde{\psi}}{\partial \theta} - \frac{\partial \omega}{\partial \theta}\frac{\partial \tilde{\psi}}{\partial \xi} + \frac{2}{Re}\left(\frac{\partial^2 \omega}{\partial \xi^2} + \frac{\partial^2 \omega}{\partial \theta^2}\right)\right], \tag{6}$$

$$\nabla^2 \tilde{\psi} = \mathrm{e}^{2\xi}\,\omega, \tag{7}$$

where

$$\nabla^2 \tilde{\psi} = \frac{\partial^2 \tilde{\psi}}{\partial \xi^2} + \frac{\partial^2 \tilde{\psi}}{\partial \theta^2}.$$

2.1. Initial conditions

The cylinder, being suddenly started from the rest, has the following initial conditions:

$$\tilde{\psi} = 0 \quad \text{and} \quad \omega = 0 \ \text{ at } \ t = 0. \tag{8}$$

2.2. Boundary conditions

**For* $\xi \to 0$

The cylinder, being deformable, has velocity components at the wall of

$$u_1 = \frac{\partial a}{\partial t_1} \quad \text{and} \quad v_1 = 0,$$

i.e. taking into account (3),

$$v_1 = \frac{\partial \psi_1}{\partial r_1} = 0 \Rightarrow \psi_1$$

is independent of r_1, i.e. $\tilde{\psi}$is independent of ξ;

$$u_1 = -\frac{1}{r_1}\frac{\partial \psi_1}{\partial \theta} = \frac{\partial a}{\partial t_1}, \quad \text{whence} \quad \tilde{\psi} = -\frac{\theta}{a_0}\frac{\partial a}{\partial t}.$$

It results from the previous equation that $\tilde{\psi}$ is a non-uniform function on the surface of the cylinder. Hence, a uniform function ψ is introduced as

$$\psi = \tilde{\psi} + \frac{\theta}{a_0}\frac{\partial a}{\partial t}. \tag{9}$$

**For* $\xi \to \infty$

The streamfunction of the flow past a deformable circular cylinder is well-known

$$\tilde{\psi} = 2\sinh(\xi_\infty)\sin(\theta) - \frac{\theta}{a_0 e^{\xi_\infty}}\frac{\partial a}{\partial t}.$$

By introducing the uniform streamfunction, the boundary condition is determined by

$$\tilde{\psi} = 2\sinh(\xi_\infty)\sin(\theta) - \frac{\theta}{a_0 e^{\xi_\infty}}\frac{\partial a}{\partial t} + \frac{\theta}{a_0}\frac{\partial a}{\partial t}. \tag{10}$$

2.3. The new system to resolve

The new system to resolve is determined by

$$\frac{\partial \omega}{\partial t} = \frac{\omega}{a}\frac{\partial a}{\partial t} + \frac{a_0}{a} e^{-2\xi} G, \tag{11}$$

$$\nabla^2 \psi = e^{2\xi}\omega, \tag{12}$$

where

$$G = \left[\frac{\partial \omega}{\partial \xi}\left(\frac{\partial \psi}{\partial \theta} - \frac{1}{a_0}\frac{\partial a}{\partial t}\right) - \frac{\partial \omega}{\partial \theta}\frac{\partial \psi}{\partial \xi} + \frac{2}{Re}\left(\frac{\partial^2 \omega}{\partial \xi^2} + \frac{\partial^2 \omega}{\partial \theta^2}\right)\right], \tag{13}$$

with the new boundary conditions

$$\psi = 0 \quad \text{for} \quad \xi = 0$$

$$\psi = 2\sinh(\xi_\infty)\sin(\theta) - \frac{\theta}{a_0 e^{\xi_\infty}}\frac{\partial a}{\partial t} + \frac{\theta}{a_0 e^{\xi_\infty}}\frac{\partial a}{\partial t} \quad \text{for} \quad \xi \to \infty$$

$$\frac{\partial \omega}{\partial t} = \frac{\omega}{a}\frac{\partial a}{\partial t} + \frac{a_0}{a} e^{-2\xi}\left[\frac{\partial \omega}{\partial \xi}\left(\frac{\partial \psi}{\partial \theta} - \frac{1}{a_0}\frac{\partial a}{\partial t}\right) - \frac{\partial \omega}{\partial \theta}\frac{\partial \psi}{\partial \xi}\right] \quad \text{for} \quad \xi \to \infty$$

and the initial symmetry of the flow, valid for all values of r, yields

$$\psi = 0 \quad \text{and} \quad \omega = 0 \quad \text{for } \theta = 0 \quad \text{and} \quad \theta = \pi. \tag{14}$$

3. FORCES ON THE BODY

The drag force may be computed as the sum of the pressure drag F_p and the friction drag F_f. The pressure drag can be determined from the vorticity flux on the cylinder surface as

$$\vec{F}_p = -\int_0^{2\pi}\left(\frac{2}{Re}\frac{\partial \omega}{\partial \xi} + \left(\frac{\partial \psi}{\partial \theta} - \frac{1}{a_0}\frac{\partial a}{\partial t}\right)\omega\right)\vec{e}_\theta \, d\theta, \tag{15}$$

while the friction drag may be computed from the vorticity on the cylinder surface as

$$\vec{F}_f = \int_0^{2\pi}\left(\frac{2\omega}{Re}\right)\vec{e}_\theta \, d\theta. \tag{16}$$

Hence, the total drag force on the body follows

$$\vec{F}_T = \vec{F}_p + \vec{F}_f \tag{17}$$

and the drag coefficient of the body is given by

$$C_D = \frac{\vec{F}_T \cdot \vec{e}_x}{U_\infty^2 a}. \tag{18}$$

4. NUMERICAL METHOD

The second-order Adams–Bashforth temporal scheme is used together with central differences in space for Equation (11) on a grid defined by $\xi_i = (i-1)\Delta\xi$, $i = 1, 2, \ldots, M$; $\theta_j = (j-1)\Delta\theta$, $j = 1, 2, \ldots, N$; $\Delta\xi = \xi_\infty/(M-1)$ and $\Delta\theta = \pi/(N-1)$. The domain is truncated in the ξ-direction at ξ_∞. As a result, the calculation of $\omega_{i,j}^{n+1}$ is given by

$$\omega_{i,j}^{n+1} = \omega_{i,j}^{n}\left[\frac{(1+A(t+\Delta t))}{(1+At)}\right] + \frac{\Delta t}{2}\left(\frac{1}{(1+At)}\right)\mathrm{e}^{-2\xi}\,(3G_{i,j}^{n} - G_{i,j}^{n-1})$$

and

$$G_{i,j} = \left(\frac{\psi_{i,j+1}-\psi_{i,j-1}}{2\Delta\theta} - \frac{1}{a_0}\frac{\partial a}{\partial t}\right)\frac{\omega_{i+1,j}-\omega_{i-1,j}}{2\Delta\xi} - \frac{\psi_{i+1,j}-\psi_{i-1,j}}{2\Delta\xi}\frac{\omega_{i,j+1}-\omega_{i,j-1}}{2\Delta\theta} + \frac{2}{Re}\left(\frac{\omega_{i-1,j}-2\omega_{i,j}+\omega_{i+1,j}}{(\Delta\xi)^2} + \frac{\omega_{i,j-1}-2\omega_{i,j}+\omega_{i,j+1}}{(\Delta\theta)^2}\right),$$

where the superscript 'n' characterizes the time discretization.

By using the following expansions for ψ and ω:

$$\psi(\xi, \theta, t) = \sum_{n=1}^{N} f_n(\xi, t)\sin(n\theta), \tag{19}$$

$$\omega(\xi, \theta, t) = \sum_{n=1}^{N} F_n(\xi, t)\sin(n\theta), \tag{20}$$

Equation (12) becomes

$$\int_0^\pi \left(\frac{\partial^2\psi}{\partial\xi^2} + \frac{\partial^2\psi}{\partial\theta^2}\right)\sin(m\theta)\,\mathrm{d}\theta = \int_0^\pi \mathrm{e}^{2\xi}\sin(m\theta)\,\mathrm{d}\theta.$$

Orthogonality of the basis and trial functions implies

$$\frac{\partial^2 f_n}{\partial\xi^2} - n^2 f_n = \mathrm{e}^{2\xi} F_n, \tag{21}$$

which defines a system of equations in Fourier space, with the following boundary conditions,

$$f_n(0, t) = 0 \quad \text{and} \quad f_n(\xi_\infty, t) = \frac{2}{\pi}\int_0^\pi \psi(\xi_\infty, \theta, t)\sin(n\theta).$$

Equation (21) is discretized in the Fourier space using central differences so that

$$f_{n,i-1} - [2 + (\Delta\xi)^2 n^2] f_{n,i} + f_{n,i+1} = (\Delta\xi)^2\,\mathrm{e}^{2\xi_i} F_{n,i}. \tag{22}$$

Equation (22) defines a tridiagonal system of equations. An inverse Fourier transform on the solution of (22) yields the corresponding solution in physical space (ψ_{ij}).

For the downstream boundary condition at infinity, an open boundary condition is established by assuming that the viscous–diffusive effect is negligible; then the vorticity equation will be

$$\frac{\partial\omega}{\partial t} = \frac{\omega}{a}\frac{\partial a}{\partial t} + \frac{a_0}{a}\,\mathrm{e}^{-2\xi}\left[\frac{\partial\omega}{\partial\xi}\left(\frac{\partial\psi}{\partial\theta} - \frac{1}{a_0}\frac{\partial a}{\partial t}\right) - \frac{\partial\omega}{\partial\theta}\frac{\partial\psi}{\partial\xi}\right], \tag{23}$$

where

$$\frac{\partial \tilde{\psi}}{\partial \theta} = \frac{1}{2\Delta\theta}(\psi(\xi_\infty, \theta + \Delta\theta) - \psi(\xi_\infty, \theta - \Delta\theta)) - \left(\frac{1}{a_0}\frac{\partial a}{\partial t}\right),$$

$$\frac{\partial \omega}{\partial \theta} = \frac{1}{2\Delta\theta}(\omega(\xi_\infty, \theta + \Delta\theta) - \omega(\xi_\infty, \theta - \Delta\theta))$$

$$\frac{\partial \tilde{\psi}}{\partial \xi} = \frac{1}{\Delta\xi}(\psi(\xi_\infty, \theta) - \psi(\xi_\infty - \Delta\xi, \theta)),$$

$$\frac{\partial \omega}{\partial \xi} = \frac{1}{\Delta\xi}\left(\frac{\omega^{n+1}(\xi_\infty, \theta) + \omega^{n-1}(\xi_\infty, \theta)}{2} - \omega(\xi_\infty - \Delta\xi, \theta)\right).$$

This condition is similar to the so-called 'radiant Sommerfeld condition'.

It remains only to determine the surface vorticity over the cylinder (equivalently, the boundary condition for Equation (11)). Equation (12) at $\xi = 0$ is

$$\frac{\partial^2 \psi}{\partial \xi^2} = \omega(0, \theta, t). \tag{24}$$

A Taylor expansion yields a second-order equation for $\omega(0, \theta, t)$,

$$\omega_{i,j} = \frac{1}{2(\Delta\xi)^2}(-7\psi_{1,j} + 8\psi_{2,j} - \psi_{3,j}). \tag{25}$$

So, similar to Hakizumwami [34], the sequence of the numerical calculations is the following:

1. Initially, consider an irrotational flow, $\omega(\xi, \theta, 0) = 0$.
2. Do a Fourier sine transform on ω. Do a Fourier sine transform on the boundary condition at infinity. Solve the Poisson equation for the streamfunction in the Fourier space. Take the inverse Fourier sine transform of the solution.
3. The solution in the previous step is used to update the vorticity along of the cylinder surface to satisfy the no-slip condition.

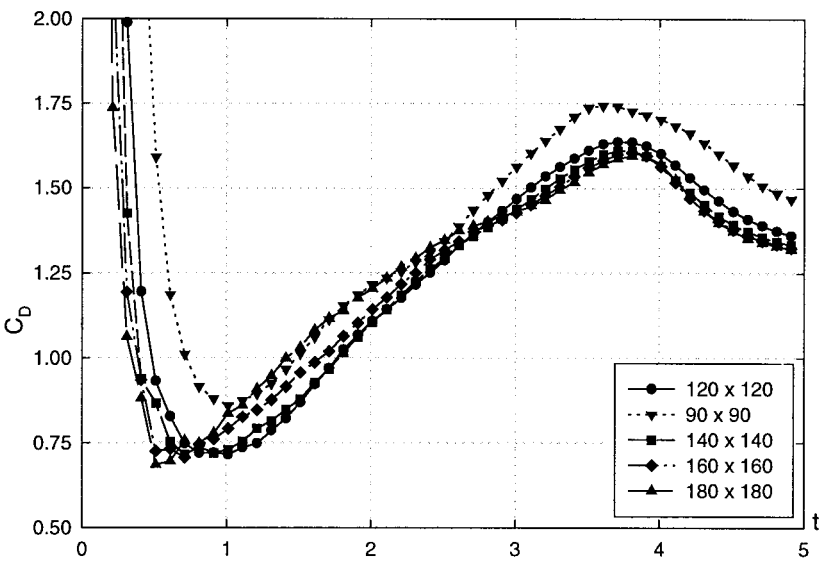

Figure 2. Drag coefficient of an impulsively started deformable cylinder at $Re_0 = 3000$ for different grid sizes.

4. Construct new values for the vorticity by solving the transport equation, with appropriate time marching.
5. Repeat all steps from step 2.

5. RESULTS FOR $Re_0 = 550$ AND $Re_0 = 3000$

First of all, if a circular cylinder was deformed (with a radius growing or reducing in time) in a fluid at rest, the flow streamlines would be rectilinear. To set impulsively either growing or

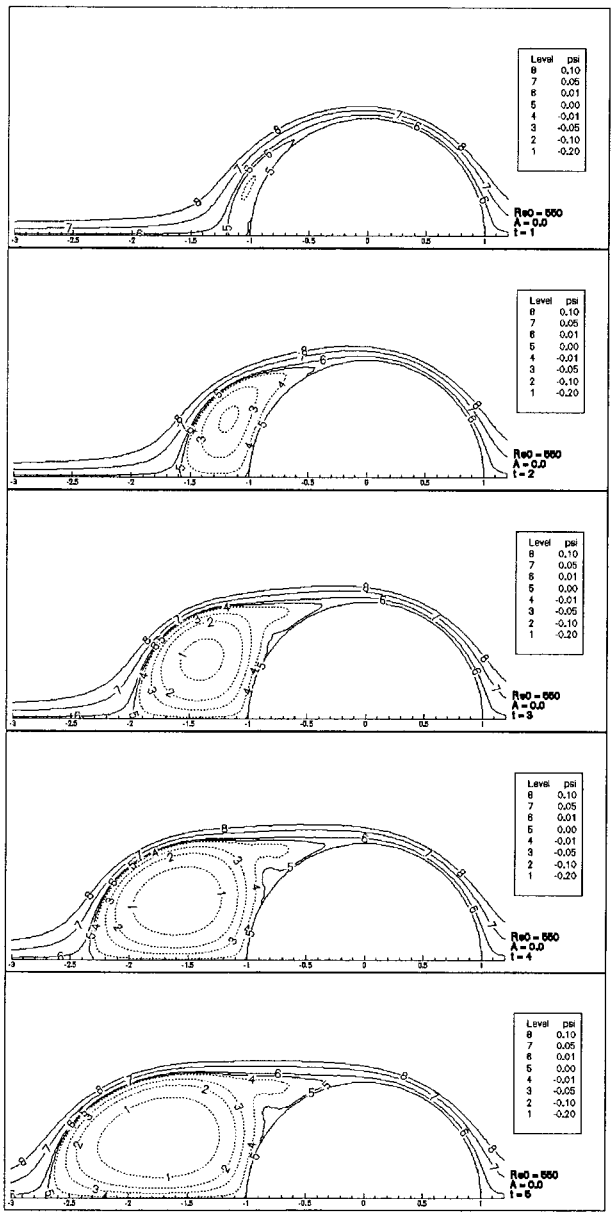

Figure 3. Evolution of instantaneous streamlines for $Re_0 = 550$ and $A = 0$.

reducing circular cylinder in a rectilinear translation would cause some backward deviations of the streamlines.

Now, the flow structure around an impulsively started and uniformly deforming circular cylinder for $Re_0 = 550$ and $Re_0 = 3000$ will be looked at.

After using many grid sizes for the numerical calculations, due to accuracy reasons, only the following ones will be used: 90×90 for $Re_0 = 550$ and 120×120 for $Re_0 = 3000$, with the time step $\Delta t = 0.01$ and $\xi_\infty = 1.6094$. Namely, for the relatively large value $Re_0 = 3000$, for instance, Figure 2 shows a good grouping together of all results beyond the grid size 120×120.

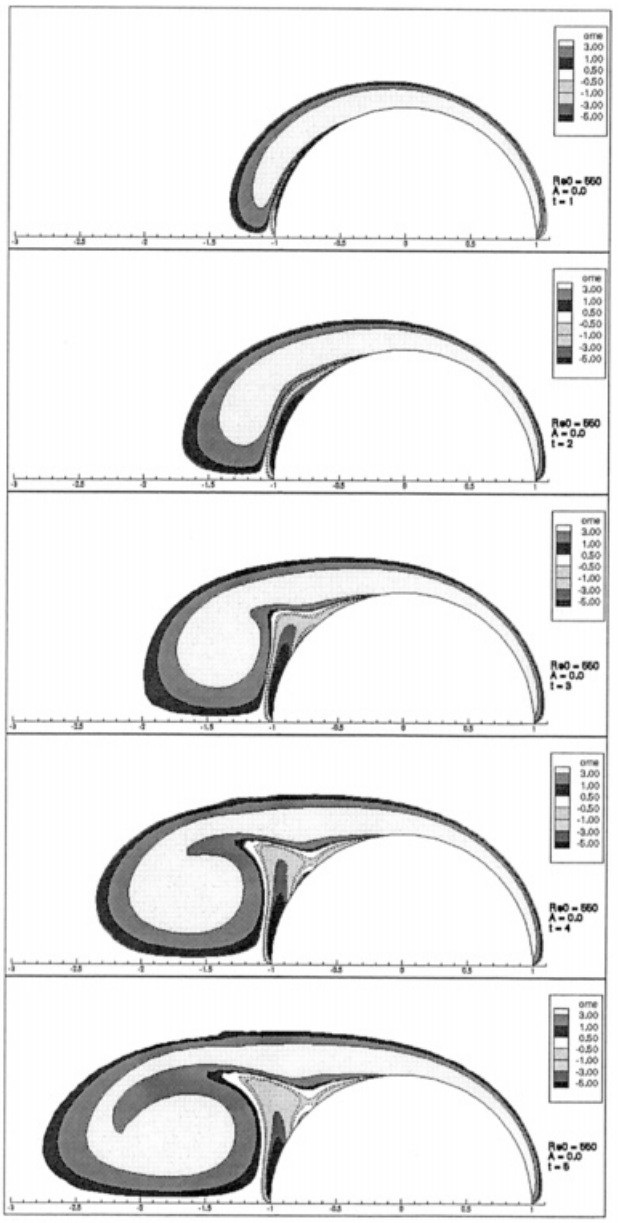

Figure 4. Evolution of equi-vorticity contour for $Re_0 = 550$ and $A = 0$.

5.1. The flow structure

5.1.1. Non-deformable cylinder. The flow structure past an impulsively started non-deforming circular cylinder is complex. The streamline history and equi-vorticity lines of the flow fields are presented in Figures 3–6.

Beside the primary vortex, the appearance of a small secondary region can be observed. The streamline patterns show the appearance of a secondary vortex at $t = 3$ for $Re_0 = 550$ (Figure 3) and for $Re_0 = 3000$ (Figure 5). The secondary vorticity is also visible in the vorticity plots

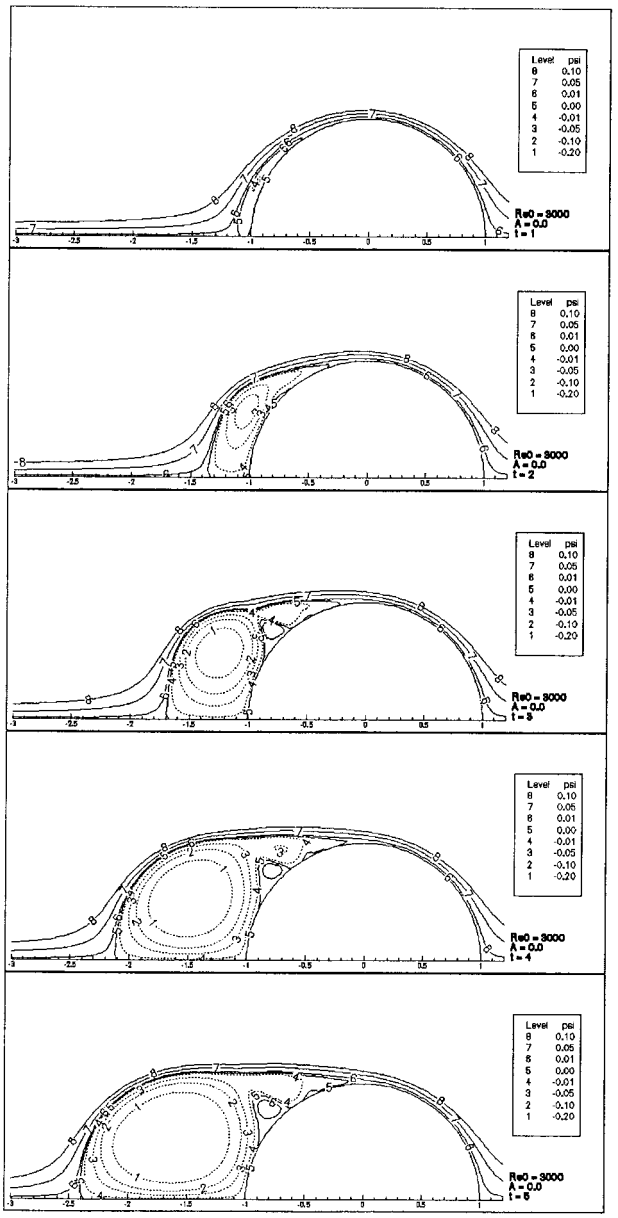

Figure 5. Evolution of instantaneous streamlines for $Re_0 = 3000$ and $A = 0$.

at $t = 2$ for $Re_0 = 550$ (Figure 4) and for $Re_0 = 3000$ (Figure 6). It is the so-called α-phenomenon [33]. The secondary vorticity remains confined after its initial appearance. Its evolution is mainly affected by the dynamics of the primary vortex. As the secondary vortex grows, it penetrates the primary vortex before cutting the link between the primary vortex and the body surface (Figures 5 and 6).

The interplay of primary and secondary vorticities is manifested in the drag curve. After its initial drop, the appearance and growth of the secondary vortex increases the drag coefficient

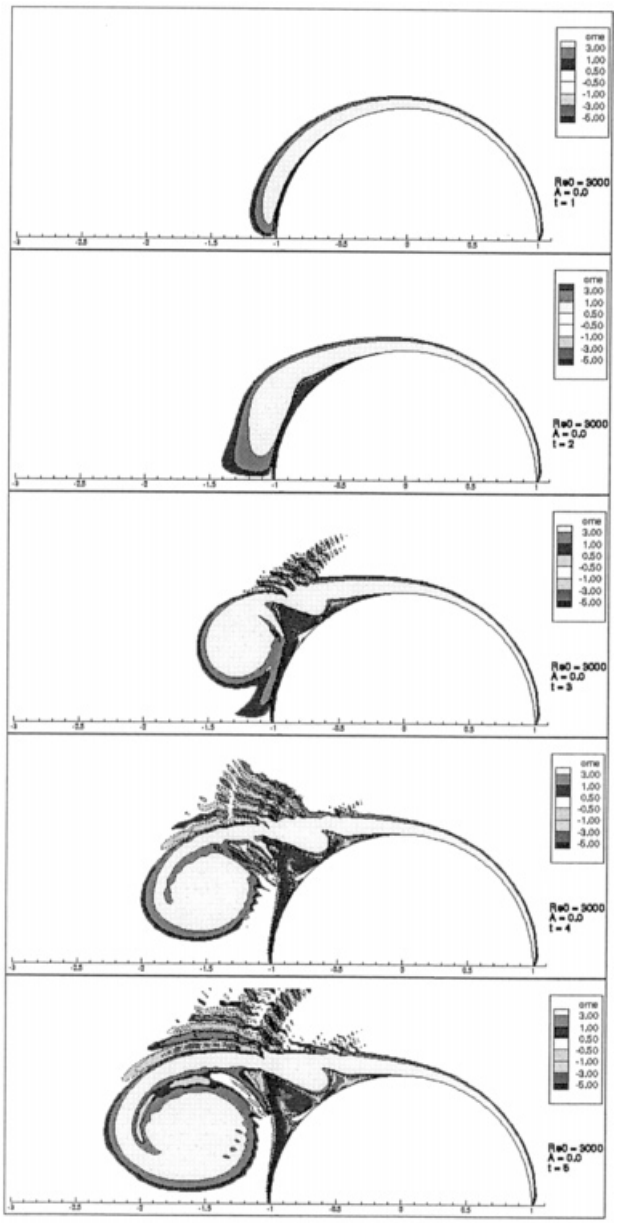

Figure 6. Evolution of equi-vorticity contour for $Re_0 = 3000$ and $A = 0$.

as the primary vortex is pushed outwards. This increase reaches a maximum at $t = 3$ for $Re_0 = 550$ (Figure 7) and at $t = 3.5$ for $Re_0 = 3000$ (Figure 8), beyond which the strength and the size of the secondary vortex are reduced, whereas the primary vortex is further convected by the free-stream velocity. The drag decays to its steady state value while symmetry persists.

Finally, the similarity of the present results concerning both evolution of time history of the surface vorticity and the streamlines for $Re_0 = 3000$ (Figures 5 and 14) with those previously obtained numerically [21] may be observed. One can also observe the similarity of the present results concerning the evolution of time history of the drag coefficient ($< 3\%$) for $Re_0 = 550$ with those previously obtained in [26]. In contrast, comparison with the results of [26], for $Re_0 = 3000$, there are some differences at early times (the minimum of the drag coefficient is equal to nearly 0.35 in [26] and 0.70 in the present work), probably because of the different grid sizes and of the fact that in the present study, an irrotationnal flow was used as an initial condition.

5.1.2. Deforming circular cylinder: $a = a_0(1 + At)$. To set impulsively a growing circular cylinder ($A > 0$) in a rectilinear translation causes a backward deviation of streamlines issued from the body surface. This deviation leads to some new phenomena beside those already announced before in the non-deformable case. As a matter of fact, the growing radius pushes the primary vortex away from the cylinder surface, renders the secondary vortex much stronger and it will be able to push the primary vortex away from the cylinder. One can also see that the so-called α-phenomenon is established before $t = 3$ for $Re_0 = 550$ (Figure 9) and for $Re_0 = 3000$ (Figure 10).

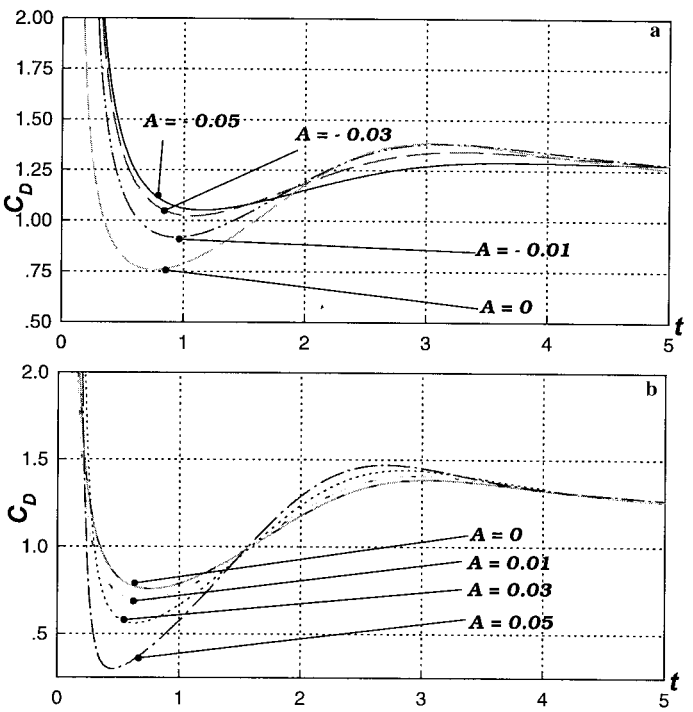

Figure 7. (a) Drag coefficient of an impulsively started reducing cylinder at $Re_0 = 550$; (b) drag coefficient of an impulsively started growing cylinder at $Re_0 = 550$.

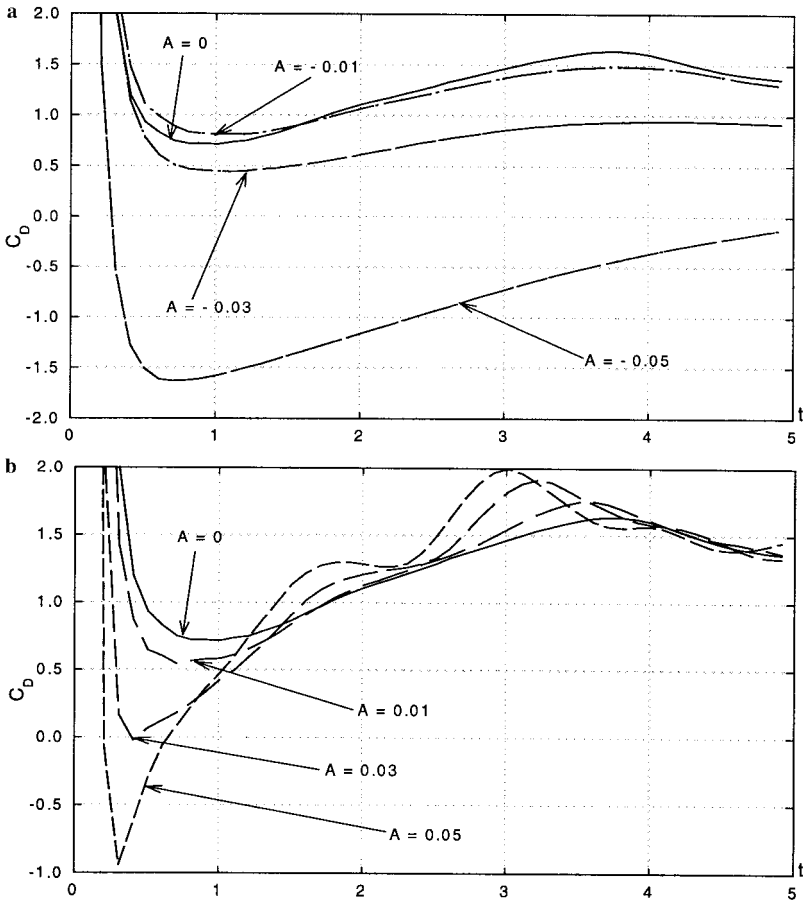

Figure 8. (a) Drag coefficient of an impulsively started reducing cylinder at $Re_0 = 3000$; (b) drag coefficient of an impulsively started growing cylinder at $Re_0 = 3000$.

In the case of a reducing radius ($A < 0$), there is another new flow phenomenon behind the cylinder. In Figures 11 and 12, the developments of the flow structure are given. The cylinder with a reducing radius has a tendency to attract the fluid towards its surface. So, the primary vortex is aspired by the cylinder and the formation of the secondary vortex is delayed.

5.2. Influence of body deformability on the drag coefficient

The following was discovered relative to the drag coefficient for a growing radius ($A > 0$). Before the primary vortex formation, the fluid pushed outwards by the cylinder creates a reaction force opposite to the drag force, in addition to the effects due to sudden translation. Therefore, the bigger the deformability factor A the stronger the reaction force, and the force ratio becomes sufficient to overpower the drag force and propel the deforming cylinder down; flow in the case of $A = 0.05$ for $Re_0 = 3000$ (Figure 8), for instance. However, the formation of primary vortex reduces the precedent effect. The primary and secondary developments increase both the wake behind the cylinder and the drag force as a consequence (Figure 7(b) and Figure 8(b)). One may also observe (Figure 7(b) and Figure 8(b)), the bigger the deformability factor A the stronger the secondary vortex, cutting more rapidly, the link

between the primary vortex and the cylinder, thus the drag coefficient decreases (Figure 7(b) and Figure 8(b)).

For a reducing radius, it can be seen that initially the drag coefficient increases slightly for $Re_0 = 550$ independently of A, also for $Re_0 = 3000$ if A is between 0 and -0.01 (Figure 7(a) and Figure 8(a)). For $Re_0 = 550$, this fact is due to the formation of the primary vortex that is not so strong as to follow the surface cylinder. For $Re_0 = 3000$, the effect of body deformation is still insufficient to modify the dynamics of formation and development of primary and secondary vortices when $A > -0.01$. On the contrary, for $A < -0.01$ and $Re_0 = 3000$ (Figure 8(a)), the fluid attracted by the cylinder turns around the primary vortex, which is very strong, pushing the cylinder. The bigger the absolute value of the deformability

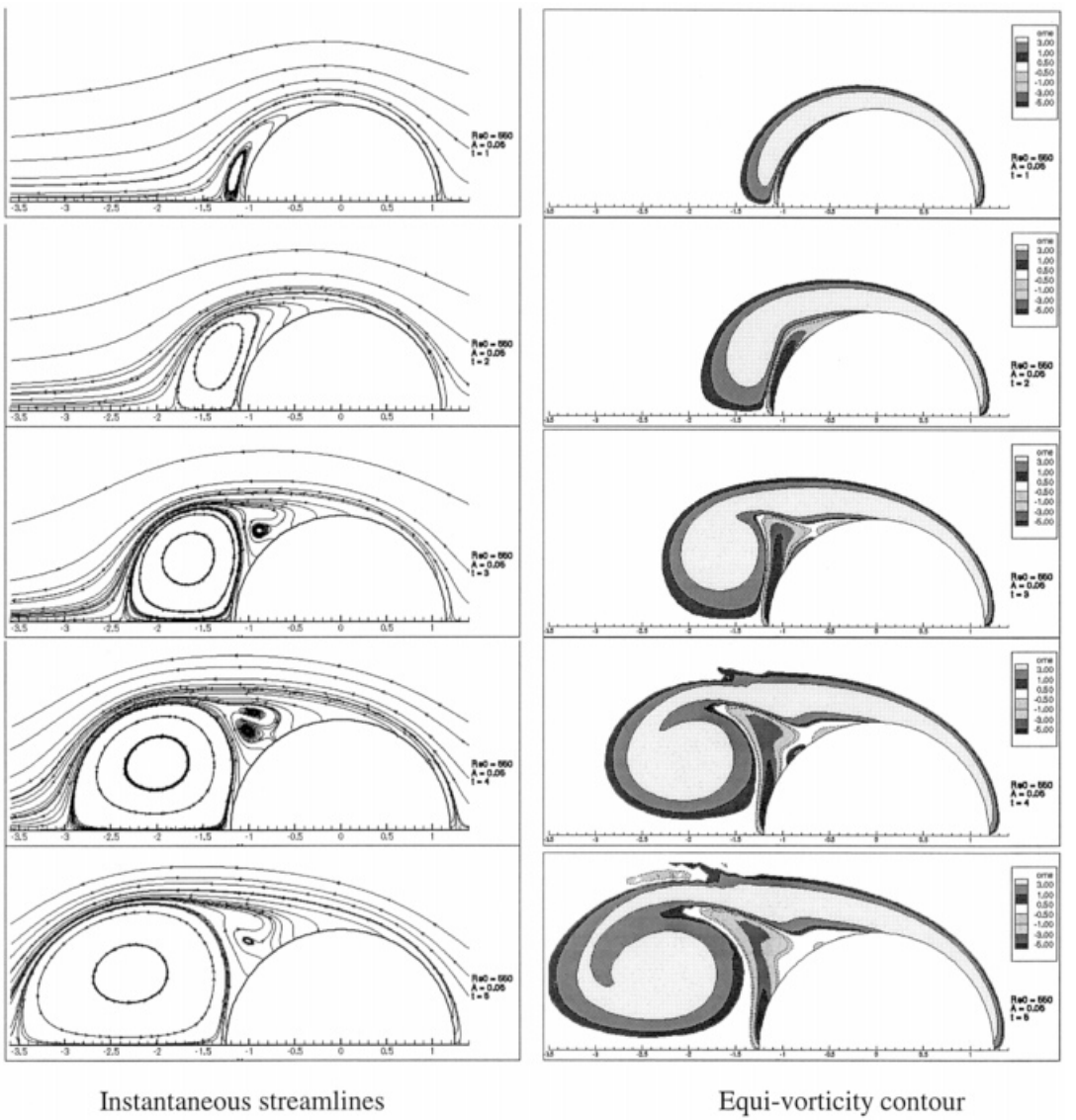

Figure 9. Evolution of the flow structure for $Re_0 = 550$ and $A = 0.05$.

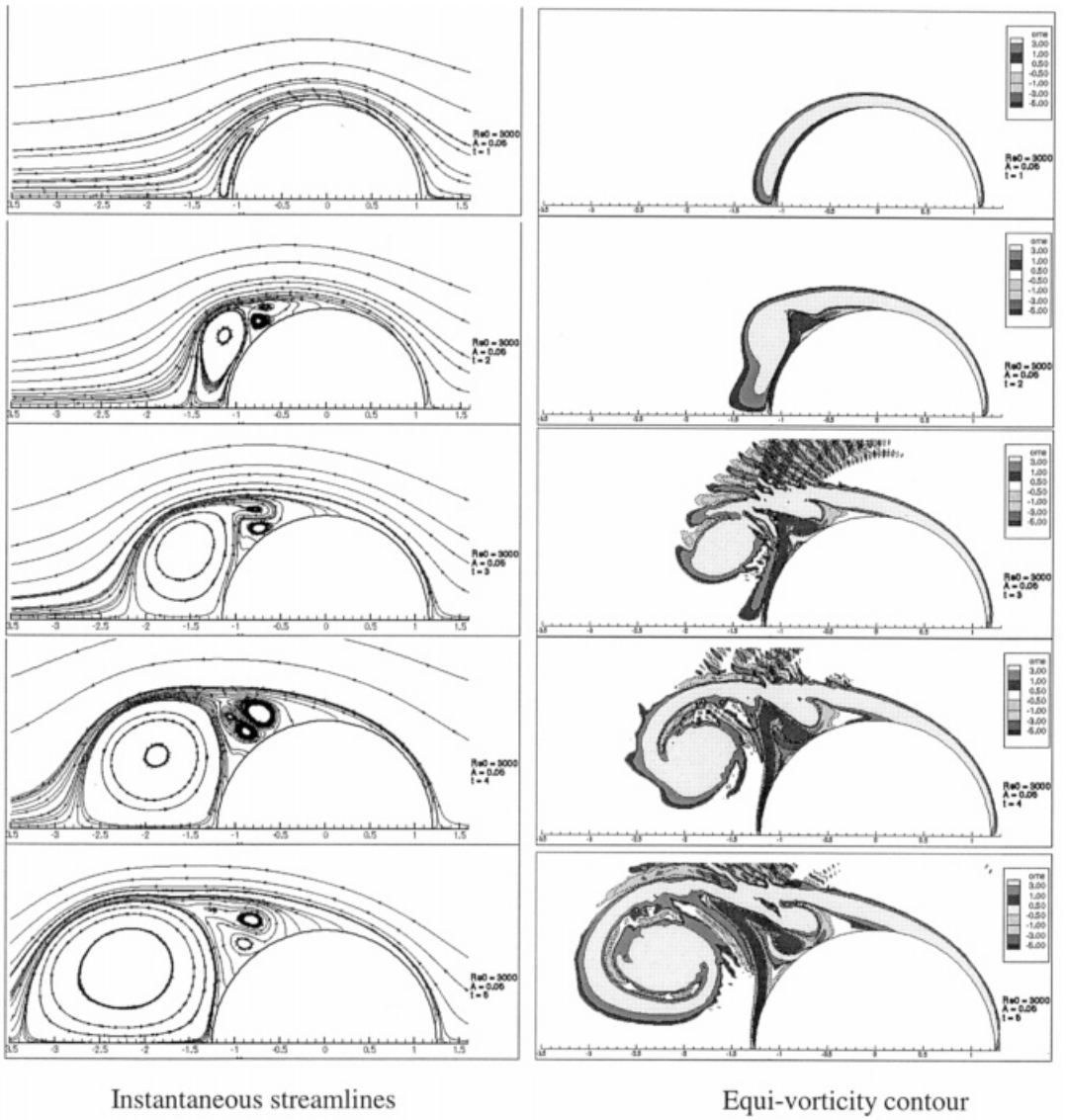

Figure 10. Evolution of the flow structure for $Re_0 = 3000$ and A = 0.05.

factor A, the more important the reduction of the drag coefficient. Then, for both Reynolds numbers, the formation and development of primary vortex increases the drag coefficient but less rapidly than in the case of non-deformable cylinder (Figures 7(a) and 8(a)).

5.3. Influence of body deformability on the boundary layer separation

The curves of vorticity on the surface of the cylinder show (Figures 13 and 14) the following: the augmentation of the radius advances the boundary layer separation, similar to the wall-injection effect, while the reduction of the radius delays the boundary layer separation as in the case of the wall-suction control.

6. CONCLUSIONS

The present numerical simulation is concerned with the analysis of unsteady separated flow at early times around the impulsively started uniformly deforming circular cylinder for the Reynolds numbers $Re_0 = 550$ and $Re_0 = 3000$. Firstly, all the results including the α-p phenomenon, previously detected either numerically or by experimental visualization, have been reproduced in detail in the preliminary non-deformable case. Then, the interaction between vortical structures and deformable walls, and their effect on the drag force experienced by the body, have been studied. The interplay of these primary and secondary vorticities, on the one hand, and the deforming surface of the cylinder, on the other hand, is the underlying

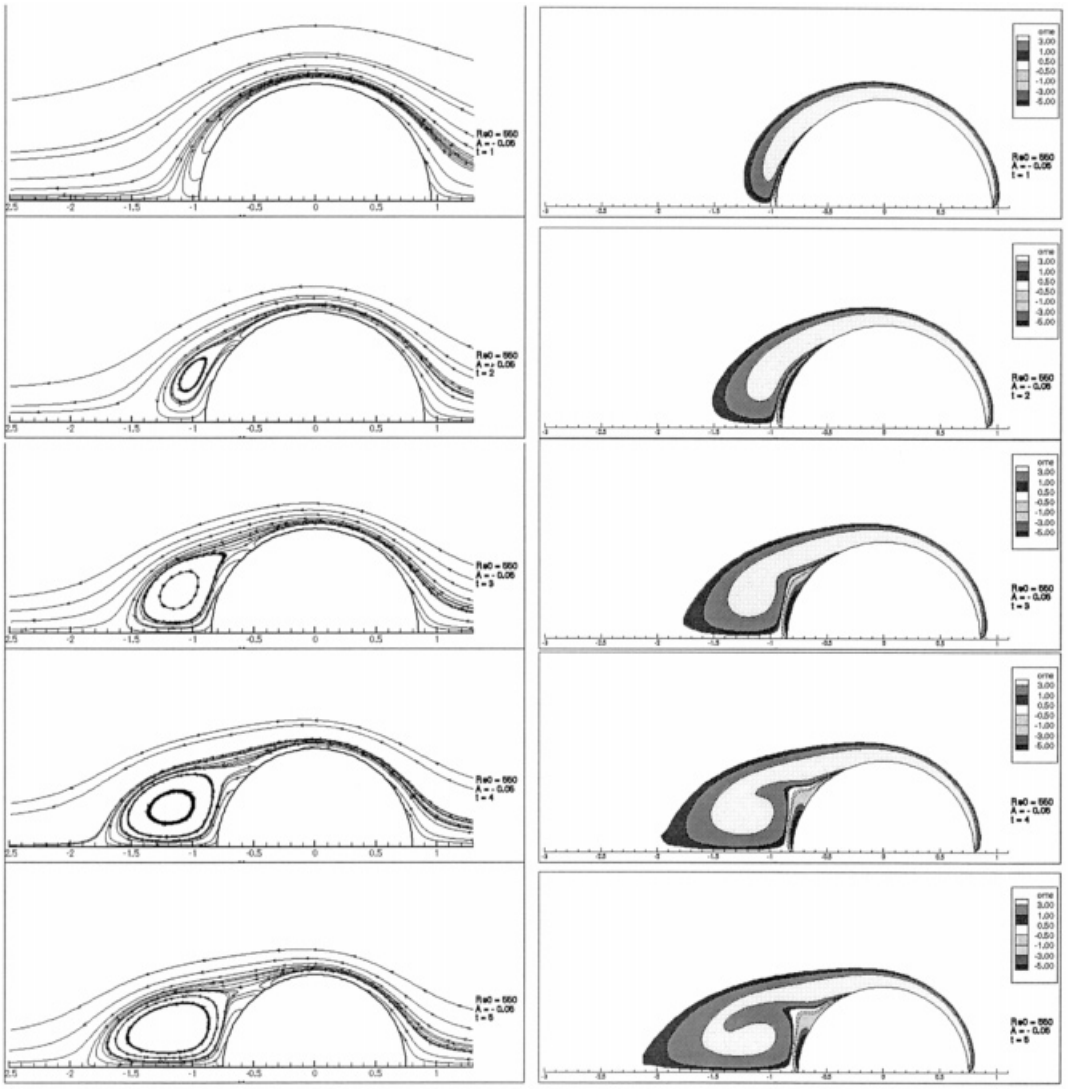

Figure 11. Evolution of the flow structure for $Re_0 = 550$ and $A = -0.05$.

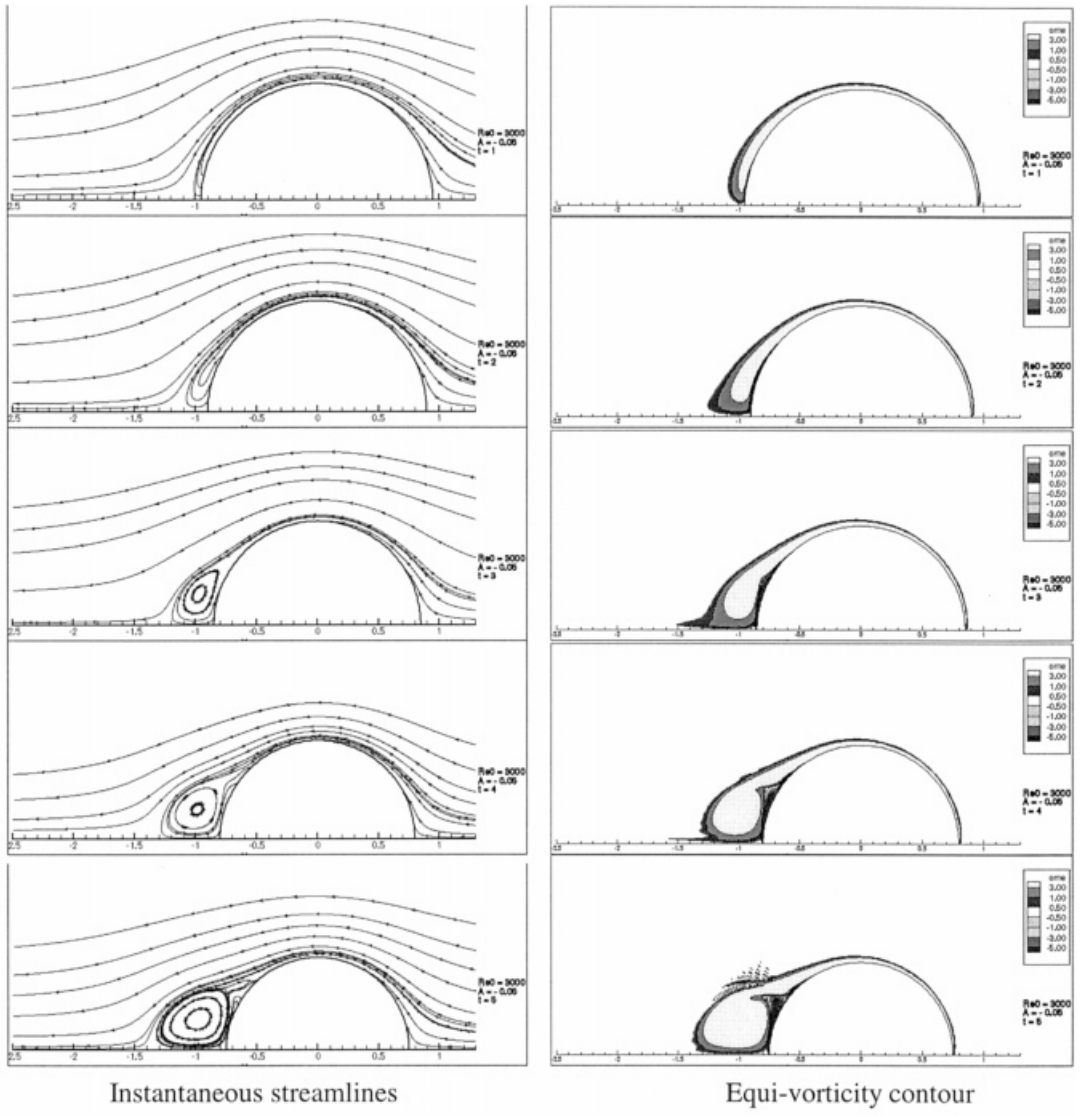

Figure 12. Evolution of the flow structure for $Re_0 = 3000$ and $A = -0.05$.

mechanism for drag reduction and increase. In fact, it has been shown here that, in both the cases of the growing radius of the cylinder and the reducing radius of the cylinder, the body deformability factor can have a favorable effect on the drag coefficient, but for different physicals reasons. In fact, in the case of a growing radius, the favorable effect comes from the force propulsion created by the body, and in the case of a reducing radius, the favorable effect comes from the attraction of the flow backwards of the cylinder and then the attraction of the primary vortex towards the cylinder. So, the body deformability may be used as a wake control device that would favorably effect the interplay of primary and secondary vorticity, thus reducing the drag coefficient.

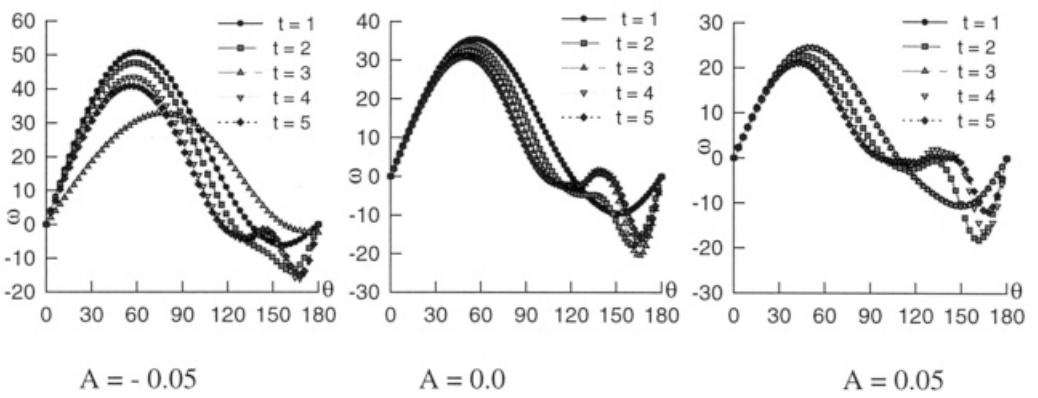

Figure 13. Vorticity on the surface of the body for $Re_0 = 550$.

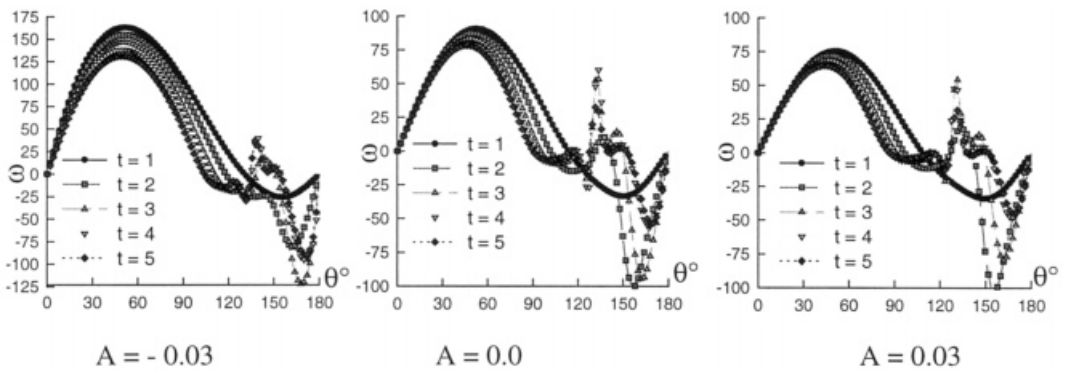

Figure 14. Vorticity on the surface of the body for $Re_0 = 3000$.

REFERENCES

1. H. Blasius, 'Grenzchichten in Flussigkeiten mit Kleiner Reiburg', *Z. Angew. Math. Phys. (Engl. trans.)*, **56**, 1 (1908).
2. S. Goldstein and L. Rosenhead, 'Boundary layer growth', *Proc. Camb. Philos. Soc.*, **32**, 392 (1936).
3. H. Schuh, 'Calculation of unsteady boundary layers in two-dimensional laminar flow', *Z. Flugwiss.*, **1**, 122 (1953).
4. H. Wundt, 'Wachstum der laminaren grenzschicht an schrag angestromten Zelindern bei Anfahrt aus der Ruhe', *Ing.-Arch. Berlin*, **23**, 212 (1955).
5. E.J. Watson, 'Boundary layer growth', *Proc. R. Soc. Lond.*, **A231**, 104 (1955).
6. X. Wang and C. Dalton, 'Numerical solutions for impulsively started and decelerated viscous flow past a circular cylinder', *Int. J. Numer. Methods Fluids*, **12**, 383–400 (1991).
7. W.M. Collins and S.C.R. Dennis, 'The initial flow past an impulsively started circular cylinder', *Q. J. Mech. Appl. Math.*, **26**, 53 (1973).
8. W.M. Collins and S.C.R. Dennis, 'Flow past an impulsively started circular cylinder', *J. Fluid Mech.*, **60**, 105 (1973).
9. M. Bar-Lev and H.T. Yang, 'Initial flow field over an impulsively started circular cylinder', *J. Fluid Mech.*, **72**, 625–647 (1975).
10. J. Jovanovic, R. Askovic and R. Djuric, 'Approximations supérieures dans la theorie de la couche limite instationnaire et leur traitement paramétrique', *GAMM-Tagung 1978, Brussels, ZAMM59*, 1979, pp. 240–243.
11. A. Thom, 'The flow past circular cylinders at low speeds', *Proc. R. Soc. Lond.*, **A141**, 651 (1933).
12. R.B. Payne, 'Calculations of unsteady viscous flow past a circular cylinder', *J. Fluid Mech.*, **4**, 81 (1958).
13. M. Kawaguti and P.C. Jain, 'Numerical study of a viscous fluid past a circular cylinder', *J. Phys. Soc. Jpn.*, **21**, 2055 (1966).
14. J.S. Son and T.J. Hanratty, 'Numerical solution of the flow around a cylinder at Reynolds number of 40, 200, 500', *J. Fluid Mech.*, **35**, 369 (1969).

15. P.C. Jain and K.S. Rao, 'Numerical solution of unsteady viscous incompressible fluid flow past a circular cylinder', *Phys. Fluids Suppl.*, **12**, 57 (1969).
16. D.C. Thoman and A.A. Szewczyk, 'Time-dependent viscous flow over a circular cylinder', *Phys. Fluids Suppl.*, **12**, 76 (1969).
17. S.C.R. Dennis and A.N. Staniforth, 'A numerical method for calculating the initial flow past a cylinder in a viscous fluid', in M. Holt (ed.) *Proc. 2nd Int. Conf. on Numerical Methods in Fluid Dynamics*, *Lecture Notes in Physics*, vol. 8, Springer, Berlin, 1971, p. 343.
18. V.A. Patel, 'Time dependent solution of viscous incompressible flow a circular cylinder', *Comp. Fluids*, **4**, 13 (1976).
19. O. Daube and Ta Phuoc Loc, 'Etude numerique d'écoulements instationnaires de fluide visqueux incompressible autour de corps profilé par une methode combiné d'ordre $0(h^2)$, $0(h^4)$', *J. Mec.*, **17**, 651 (1978).
20. Ta Phuoc Loc, 'Numerical analysis of unsteady secondary vortices generated by an impulsively started circular cylinder', *J. Fluid Mech.*, **100**, 111 (1980).
21. Ta Phuoc Loc and R. Bouard, 'Numerical solution of the early stage of the unsteady viscous flow around a circular cylinder: a comparison with experimental visualisation and measurements', *J. Fluid Mech.*, **160**, 93 (1985).
22. Y. Lecointe and J. Piquet, 'On the use of several compact methods for the study of the incompressible viscous flow around a circular cylinder', *Comp. Fluids*, **12**, 255–280 (1984).
23. X. Wang and C. Dalton, 'Numerical solution for impulsively started and decelerated viscous flow past a circular cylinder', *Int. J. Numer. Methods Fluids*, **12**, 383–400 (1991).
24. P.A. Smith and P.K. Stansby, 'Impulsively started flow around a circular cylinder by the vortex method', *J. Fluid Mech.*, **194**, 45–77 (1988).
25. C.C. Chang and R.L. Chern, 'A numerical study of flow around an impulsively started circular cylinder by a deterministic vortex method', *J. Fluid Mech.*, **233**, 243–263 (1991).
26. P. Koumoutsakos and A. Leonard, 'High-resolution simulations of the flow around an impulsively started cylinder using vortex method', *J. Fluid Mech.*, **296**, 1–38 (1995).
27. J.P. Christiansen, 'Vortex methods for flow simulation', *J. Comput. Phys.*, **13**, 363 (1973).
28. C.R. Anderson and M. Reider, 'Investigation of the use of Prandtl/Navier–Stokes equation procedures for two-dimensional incompressible flows', *CAM Rep. 93-02*, Department of Mathematics, UCLA, CA, 1993.
29. J.-Z. Wu, X. Wu, H. Ma and J.M. Wu, 'Dynamic vorticity condition: theory and numerical implementation', *Int. J. Numer. Fluids*, **19**, 905–938 (1994).
30. W. Prandtl, 'The magnus effect and wind powered ships', *Wissenschaften* **13**, 93–108 (1925).
31. H. Honji and S. Taneda, 'Unsteady flow past a circular cylinder', *J. Phys. Soc. Jpn.*, **27**, 1968 (1969).
32. S. Taneda, 'Visualisation experiments on unsteady viscous flows around cylinders and plates', in E.A. Eichelbrenner (ed.), *Recent Research on Unsteady Boundary Layers*, vol. 2, Quebec Laval University, Quebec, 1972.
33. R. Bouard and M. Coutanceau, 'The early stage of development of the wake behind an impulsively started cylinder for $40 < Re < 10^4$', *J. Fluid Mech.*, **101**, 583 (1980).
34. B.K. Hakizumwami, 'High Reynolds number flow past an impulsively started circular cylinder', *Comput. Fluids*, **7**, 895 (1994).

